Articles in PresS. J Neurophysiol (March 15, 2017). doi:10.1152/jn.00278.2016

Visual and presaccadic activity in area 8Ar of the macaque monkey lateral prefrontal cortex

Kelly R. Bullock[1,4], Florian Pieper[2], Adam J. Sachs[3], and Julio C. Martinez-Trujillo[4]

[1] Department of Physiology, McGill University, Montreal, Canada; [2] Department of Neurophysiology and Pathophysiology, University Medical Center Hamburg-Eppendorf, Hamburg, Germany; [3] Division of Neurosurgery, Department of Surgery, The Ottawa Hospital Research Institute, The University of Ottawa, Ottawa, Canada; and [4] Robarts Research Institute, Department of Physiology and Pharmacology, Brain and Mind Institute, University of Western Ontario, London, Canada.

RUNNING HEAD

Visual and presaccadic activity in area 8A of the macaque

AUTHOR CONTRIBUTIONS

K.R.B. and J.C.M.-T. drafted the manuscript; K.R.B. analyzed data; J.C.M.-T., F.P., and A.S. designed experiment; F.P. collected data; J.C.M.-T. and A.S. performed surgeries.

CORRESPONDING AUTHOR

Julio C. Martinez-Trujillo, Western University, Faculty of Schulich School of Medicine and Dentistry, Department of Physiology and Pharmacology, 1151 Richmond Street N, Room 7239, London, ON, N6A 5B7 (Email: julio.martinez@uwo.ca) (Tel: 519-931-5777) (Fax: 519-931-5789).

ABSTRACT

Common trends observed in many visual and oculomotor-related cortical areas include retinotopically organized receptive and movement fields exhibiting a Gaussian shape and increasing size with eccentricity. These trends are demonstrated in the frontal eye fields (FEF), many visual areas, and the superior colliculus (SC), but have not been thoroughly characterized in prearcuate area 8Ar of the prefrontal cortex. This is important since area 8Ar, located anterior to the FEF, is more cytoarchitectonically similar to prefrontal areas than premotor areas. Here we recorded the responses of 166 neurons in area 8Ar of two male macaques while the animals made visually guided saccades to a peripheral sine-wave grating stimulus positioned at one of 40 possible locations (8 angles along 5 eccentricities). To characterize the neurons' receptive and movement fields, we fit a bivariate Gaussian model to the baseline-subtracted average firing rate during stimulus presentation (early and late visual epoch) and prior to saccade onset (presaccadic epoch). 121/166 neurons showed spatially selective visual and presaccadic responses. Of the visually selective neurons, 76% preferred the contralateral visual hemifield, whereas 24% preferred the ipsilateral hemifield. The angular width of visual and movement-related fields scaled positively with increasing eccentricity. Moreover, responses of neurons with visual receptive fields were modulated by target contrast exhibiting sigmoid tuning curves that resemble those of visual neurons in upstream areas such as MT and V4. Finally, we found that neurons with receptive fields at similar spatial locations were clustered within the area; however, this organization did not appear retinotopic.

Keywords: prefrontal cortex, receptive fields, target selection, clustering, saccades

NEW & NOTEWORTHY

We recorded the responses of neurons in lateral prefrontal area 8Ar of macaques during a visually guided saccade task using multielectrode arrays. Neurons have Gaussian-shaped visual and movement fields in both visual hemifields with a bias towards the contralateral hemifield. Visual neurons show contrast response functions with sigmoid shapes. Visual neurons tend to cluster at similar locations within the cortical surface, however this organization does not appear retinotopic.

INTRODUCTION

Several studies have suggested that the lateral prefrontal cortex (LPFC) plays a role in cognitive control of visually guided oculomotor behavior (Barone and Joseph 1989), encoding rules for goal-directed behavior (Wise et al. 1996; Miller 1999; Wallis et al. 2001), adaptive response strategies (Genovesio et al. 2005), attention (Everling et al. 2002; Rossi et al. 2007; Lennert and Martinez-Trujillo 2011; Lennert and Martinez-Trujillo 2013; Tremblay et al. 2015), working memory (Miller 1999; Mendoza-Halliday et al. 2014), decision-making (Kiani et al. 2014; Seo et al. 2007) and the ability to suppress automatic behavioral responses (Wegener et al. 2008).

In particular, area 8Ar—the region of the LPFC between the arcuate sulcus and the posterior tip of the principal sulcus (Preuss and Goldman-Rakic 1991; Petrides and Pandya 1999), just anterior to the Frontal Eye Fields (FEF) (Stanton et al. 1989) —is a cortical area that likely plays a role in visuomotor integration within the saccade generation network on the basis of its *connectivity* and *response properties*. Namely, area 8Ar shares connections with parietal areas responsible for visuospatial processing including areas LIP and 7 (Barbas and Mesulam 1981; Andersen et al. 1990; Petrides and Pandya 1999; Schall et al. 1995b), and is heavily

interconnected with the neighboring areas in the LPFC such as area 9/46, and with the FEF (Stanton et al. 1993; Yeterian et al. 2012).

Topography—the orderly projection of sensory receptors onto the cortex—is an organizing principle preserved throughout much of the saccade generation network. For instance, rough retinotopic maps are described in visual areas V4 (Gattass et al. 1988) and MT (Van Essen et al. 1981; Ungerleider and Desimone 1986; Maunsell and Van Essen 1983), and frontal areas such as FEF (Bruce et al. 1985; Stanton et al. 1989). Areas of the parietal cortex such as LIP (Blatt et al. 1990, Ben Hamed et al. 2001; Arcaro et al. 2011) are also thought to have topographic organization; however, this issue has not been settled. In addition to retinotopy of visually selective neurons, microstimulation of the FEF in macaques has revealed a topographic organization of saccade amplitude, but not direction (Bruce et al. 1985; Stanton et al. 1989). When stimulated, the dorsomedial portion (in the superior limb of the AS) of FEF produces large-amplitude (15-20^{o}) saccades, and the ventrolateral portion (in the inferior limb of the AS) elicits small-amplitude saccades (Bruce et al. 1985). However, it is less clear to what extent the more anterior and superficially located area 8Ar contains a topographic representation of visual and oculomotor space.

Neurons in visual and oculomotor areas respond preferentially to stimuli shown at certain locations in visual space or prior to saccades toward such locations. This spatially selective firing delineates receptive fields (RFs), the location at which a visual stimulus evokes a firing rate above baseline, and movement fields (MFs), the saccade target location eliciting firing rates above baseline. The baseline is defined as the firing rate when the animal is not engaged in a specific task and visual targets are not present. Suzuki and Azuma (1983) report isocontour lines of RF size and eccentricity within area 8Ar. They found that RF size and eccentricity increase as

one moves medially from the inferior arcuate sulcus towards the posterior tip of the principal sulcus. They also observed that RF size, but not eccentricity, increases as one move anteriorly from the knee of the arcuate sulcus towards the principal sulcus (Suzuki and Azuma 1983). However, these analyses have not been replicated, and to our knowledge, no study to date has examined the response properties of RFs and MFs in area 8Ar in detail.

Here, we recorded neural responses from the left area 8Ar of two macaques while the subjects performed a visually guided saccade task using a multielectrode array (MEA). We systematically characterized the RF and MF properties of 8Ar neurons in terms of their spatial extent across eccentricity and contrast sensitivity, and investigated the relationship between cortical location and spatial representation. We found that 76% of the recorded neurons preferred the contralateral visual hemifield, whereas 24% preferred the ipsilateral hemifield. Moreover, neurons with RFs and MFs at similar spatial positions were clustered within the same region of the cortical surface.

METHODS

Subjects and ethics statement

All procedures were carried out pursuant to the Canadian Council for Animal Care guidelines and pre-approved by the McGill University Animal Care Committee. Recordings were made from the dorsolateral prefrontal area 8Ar (Petrides and Pandya 1999) of two adult male cynomolgus macaques (*Macaca fascicularis*), henceforth referred to as monkeys JL and F. Animals were pair-housed in large enclosures; interaction with facility personnel, treats, and toys were provided daily to enrich the environment. On experimental days fluid intake was restricted, and a juice reward was earned by the animals upon successful completion of the task. Water

intake was supplemented to guarantee animals received a minimum of 35 ml/kg/day, even if animals failed to obtain this amount during the experiment. Fresh fruits and vegetables were also provided daily. Animals were monitored for signs of distress or illness. Criteria used to define distress or illness included changes in body weight, grooming habits, and water intake, and these were recorded daily. Other physiological markers of well-being—such as blood cell count, hemoglobin, hematocrit, and kidney function—were examined quarterly. At any indication of discomfort or illness resulted in cessation of the experiment until treatment and recovery were completed, as determined by an animal welfare veterinarian.

Head-post and microelectrode array (MEA) implantation

Before the experiments, 3 head-posts were implanted on each animal; one positioned on the midline posterior to the supra-orbital ridge and two placed superior to the external occipital protuberance on the petrosal bones. The head-posts allowed for fixation of the animal's head during experimentation.

A 96 channel microelectrode array (MEA; 4mm by 4mm; Blackrock Microsystems LLC, Utah, USA) (Maynard et al. 1997; Normann et al. 1999) was implanted in the left dorsolateral prefrontal area 8Ar of each monkey—in the prearcuate gyrus between the posterior end of the principal sulcus and the knee of the arcuate sulcus (Fig. 1*A*), as detailed in Leavitt et al. 2013. Briefly, a craniotomy was made using a high-powered drill (Anspach, FL, USA) to reveal the principal and arcuate sulci. The dura was opened and the MEA inserted with an array gun (Blackrock Microsystems LLC, Utah, USA) to a depth of approximately 1-1.5 mm from the cortical surface. We performed a duraplasty using synthetic dura (Durepair, Medtronic, Inc. Minneapolis, MN, USA), and replaced and secured the bone flap with fixation plates and screws (Synthes, Inc. PA, USA). All surgical procedures were carried out under general anesthesia

administered via an endotracheal tube. Animals were fully recovered from surgery within one week.

Data collection

During the experimental session, eye-positions were tracked with an infrared eye-tracker at a sampling frequency of 500 Hz (EyeLink 1000, SR Research, Ontario, Canada) (Khayat et al. 2010). The neuronal signal was amplified via a headstage (ICS-96) for a reduced-noise signal, band-pass filtered (0.3 Hz/1-pole, 7.5 kHz/3-pole, analog) and digitized (16 bit, 1 microV per bit, sample rate of 30 kHz) using a neuronal signal processor (Cerebus, Blackrock Microsystems, Utah, USA). Spike waveforms were acquired by setting a threshold of -4 to -4.5 x the noise amplitude of the digitized, high-pass filtered raw signal.

For single unit analysis, individual neurons were isolated based on waveform properties such as peak-to-peak amplitude in principle component space using OfflineSorter (Plexon, USA). The MEA electrodes were evenly spaced along intervals of 0.4 mm and arranged into three blocks of 32 simultaneously-recorded electrodes. Each session was comprised of data collected from one of the three blocks (A, B, C) (Leavitt et al. 2013).

Task

A custom computer program recorded the behavioral data (eye signals and lever presses) and presented the visual stimuli. The screen was positioned 100 cm from the animals' eyes. A trial was initiated when the monkey held gaze position within a 2 degree window of a central fixation point (0.08 degrees^2) and pressed a lever to indicate willingness to start the trial. After fixating for 650 ms, a sine wave grating (2.5 cycles per degree, 1 degree visual angle in diameter, oriented at 90 degrees to the horizontal, luminance contrast of 3%, 5%, 10%, 20%, or 35%)

appeared at one of 40 randomly selected locations, arranged along eight polar angles in steps of 45^{o} and five eccentricities spaced in increments of 3 degrees visual angle (dva) (Fig. 1*B*). The monkey maintained central fixation for 650 ms of stimulus presentation, after which the central fixation point was extinguished, cueing the monkey to saccade to the peripheral stimulus. If the monkey initiated the saccade within 125-600 ms of the response cue, and the saccade endpoint landed within a radius of 1.25 dva of the stimulus, a juice reward was given. Fixation breaks, premature lever releases, or failing to land on the saccade target resulted in a failed trial, which was aborted without reward.

Data analysis

All data analysis was conducted with Matlab software (Mathworks, Natick, USA). Spike waveforms were stored as discreet spike event times (the nearest millisecond following threshold crossing). For single cell analysis, we recorded from a total of 166 neurons (60 in JL; 106 in F) across three sessions for each subject. In each session, we recorded from a block of 32 channels designated as blocks A, B, and C which together comprise an entire array. For monkey JL, we isolated neurons from blocks A, B, and C, and in monkey F we isolated neurons from two sessions in block B, and one from block C. Any isolated neurons with a maximum firing rate of less than 1 spike per second (Sp/s) were excluded from analysis. For topographical analysis, we used the thresholded signal on the electrodes from blocks A, B, and C for both animals in order to maximize the number of electrodes included in analysis.

For single-cell RF and MF analysis, to ensure sufficient trial numbers, we pooled across trials with the highest contrast levels (10%, 20%, and 35% contrast) and measured the average visual and movement activity of area 8Ar neurons during the *early visual* (duration 250 ms; 100 ms after stimulus onset), *late visual* (duration 250 ms; 350 ms after stimulus onset), *presaccadic*

177 (duration 100 miliseconds; immediately prior to saccade onset) epochs, and the *baseline* firing
178 rate (duration 250 ms; 250 ms after trial initiation) (Fig. 3*B*). We divided the visual epoch into
179 *early visual* and *late visual* periods to account for temporal dynamics of the visual response. The
180 peristimulus time histogram (PSTH) was computed across an average of 18 trials (SD = 7) in 50
181 milliseconds bins.

182 ## *Saccade precision and kinematics*

183 We recorded the monkeys' eye position and calculated the duration of the saccade: the
184 time from which the eye (gaze) velocity exceeded the threshold of 25 degrees/sec to when it
185 returned to that threshold. Peak velocity was considered to be the maximal velocity during a
186 saccade. Saccade endpoint location was determined as the eye position when eye movement
187 velocity returned to the saccadic velocity threshold. In order to quantify saccade precision we
188 measured the area covered by clusters of saccade endpoints around a target; only saccade
189 endpoint from hit trials were included in analysis. An ellipse was fit to the cluster of saccade
190 endpoints to a given target, using the least squares method, and its area was computed as a
191 measurement of saccade endpoint spread (Fig. 2*C*).

192 ## *Receptive and movement fields*

193 To determine whether RF and MF width scales with eccentricity, we plotted the tuning
194 curve at each eccentricity for the RFs (visual epochs) and MFs (presaccadic epoch). To obtain
195 the tuning curve at each eccentricity, we fit a Gaussian function (*equation 1*) to the activity as a
196 function of the angle *f(x)* using the nonlinear least squares method:

197 $$f(x) = a + b * e^{-\frac{1}{2}*\left(\frac{x-\mu}{\sigma}\right)^2} \quad (1)$$

where a is the baseline or intercept, b is the height or amplitude of the peak, σ is the standard deviation, and μ is the mean. To minimize error in the Gaussian model fits and to account for the circular nature of the data, tuning curves were centered on the peak or maximal response. The tuning width for a given eccentricity was determined from the standard deviation of the corresponding Gaussian function. The RF and MF width at each eccentricity (r, in dva) was considered to be the arc length (s, given in dva) subtended by the angular width of tuning (θ, in degrees) (*equation 2*).

$$s = r * \theta \tag{2}$$

To assess the spatial extent and location of the RFs (comprising early and late visual epochs) and MFs (presaccadic epoch), a 2-dimensional Gaussian function was fit to the baseline-subtracted average activity at the 40 locations, and values between stimulus locations were interpolated (linear interpolation):

$$f(x,y) = a + b * e^{-\frac{1}{2-\rho}*\left[\left(\frac{x-\mu_x}{\sigma_x}\right)+\left(\frac{x-\mu_y}{\sigma_y}\right)-\left(\frac{2*\rho*(x-\mu_x)*(y-\mu_y)}{\sigma_x*\sigma_y}\right)\right]} \tag{3}$$

where $f(x, y)$ is the response at location (x, y), a is the intercept, b is the amplitude, ρ is the correlation between x and y, and μx, μy, σx, σy are the mean and variance/width along the Gaussian in the x and y axis, respectively. The peak of the Gaussian indicates the preferred location of a given neuron. Neurons were considered tuned for a given epoch if activity at one location was significantly modulated (Kruskal-Wallis test, $P < 0.05$) with a goodness of fit (R^2) greater than 0.75 for the Gaussian model (as per Hair et al. 2012). Some units exhibited activity at one or more locations that was vigorously suppressed below baseline. We categorized any unit

with suppression of at least 50% the magnitude of the peak activation of that cell as a 'suppressed cell.' We only considered selective neurons (n = 121) in our single cell RF and MF analysis.

Contrast response functions

Visual neurons in the macaque LGN as well as areas V1 and MT have demonstrated a saturating relationship between the neural response and increasing stimulus contrast (Albrecht and Hamilton 1982; Sclar et al. 1990). However, it is still unclear how contrast is encoded in LPFC area 8Ar. We examined the response of 7 visual (tuned in early visual epoch; Kruskal-Wallis test, $P < 0.05$), 61 visuomovement (tuned in early visual and presaccadic epoch; Kruskal-Wallis test, $P < 0.05$), and 7 movement (tuned in presaccadic epoch; Kruskal-Wallis test, $P < 0.05$) neurons in response to stimuli of 3%, 5%, 10%, 20%, and 35% contrast (Contrast=ΔL/Lmin, where ΔL is the maximum minus the minimum luminance) (Michelson 1927). We included in the analysis only cells for which there were at least three trials presented at each contrast level and exhibiting a maximum firing rate across all contrast of at least 5 spikes per second. We first subtracted the baseline firing rate to determine how contrast modulates activity relative to baseline. We then fit a sigmoid function to the contrast response:

$$R = \frac{R_{max} * C^n}{C^n + C_{50}^n} + M \quad (4)$$

where $Rmax$ refers to the difference in firing rate between response at saturation, and response at lowest contrast level (M). C_{50} represents the contrast at which the activity is at half saturation, and n is the slope of the sigmoid function (Martinez-Trujillo and Treue 2002). We included only cells with a goodness of fit (R^2) greater than 0.7 (Hair et al. 2012).

Response latencies

Previous studies have observed that the distribution of interspike intervals (ISIs) in a spike train can be modelled by the Poisson distribution (Hanes et al. 1995). Poisson spike train analysis can therefore determine periods of significant neuronal activation by comparing the observed number of spikes within a given interval to the number that would be predicted if the spikes followed a Poisson distribution (the null hypothesis).

Using this analysis method, we computed a surprise index (SI), which acts as a metric of the improbability that a burst of neural activity occurs by chance. The SI is computed thus:

$$SI = -\log P \tag{5}$$

where P is the probability of a Poisson-distributed (random) spike train. The Poisson formula is as follows:

$$P = e^{-rT} \sum_{i=n}^{\infty} (rT)^i / i! \tag{6}$$

where P is the probability that a spike train with a mean firing rate (r) will contain n or more spikes in the time interval (T) (Hanes et al. 1995).

Clustering

We assessed whether the preferred location (in Cartesian coordinates) of the neurons on a given electrode displayed non-random spatial organization on the cortex. The preferred location on a given channel was defined by the location of the peak of the bivariate Gaussian fit to the baseline-subtracted thresholded activity on an electrode. We examined the coefficient of

259 determination (R^2) as a metric of goodness of fit. Only electrodes with an acceptable goodness of
260 fit ($R^2 > 0.5$) were considered for clustering analysis.

261 To determine whether similar preferred locations were anatomically clustered, we
262 utilized *Moran's I*, a measure of spatial autocorrelation (Zuur et al. 2007; Moran 1950). Moran's
263 I is defined as

264 $$I = \frac{N}{\sum i \sum j \omega ij} \frac{\sum i \sum j \omega ij (X_i - \bar{X})(X_j - \bar{X})}{\sum i (X_i - \bar{X})^2} \quad (7)$$

265 where N is the number of spatial units as indexed by i and j; X is the variable of interest; $\bar{X}$ is the
266 mean of X; and ωij is an element of a matrix of spatial weights. Moran's I ranges from -1 to +1,
267 with negative values indicating that channels with similar values are maximally mutually
268 separated and positive values indicative that similar values occupy neighboring electrodes. A
269 value of 0 indicates a random spatial relationship of values on the array.

270 # RESULTS

271 We recorded the activity of 166 neurons in the left area 8Ar of two macaque monkeys.
272 The animals correctly learned and performed the task. The performance was higher than 95% in
273 all sessions (3 sessions per subject).

274 ## *Saccade kinematics and precision*

275 Saccades made by the animals follow stereotypical kinematics rules. Namely, the duration and
276 peak (maximal) velocity of saccades scale as a function of saccade amplitude, thus following the
277 main sequence (Bahill et al. 1975). Figure 2 shows the data from monkeys JL and F. We plotted
278 the saccade duration (Fig. 2*A*) and saccade peak velocity (Fig. 2*B*) as a function of eccentricity;

both animals displayed very similar saccade kinematics. Both the mean saccade duration (Fig. 2*A*) and peak velocity (Fig. 2*B*) displayed a monotonic positive scaling with eccentricity. The saccade endpoint spread, a measure of saccadic precision, was determined at various eccentricities from the area of ellipses fit to saccade landing positions clusters around the target center position. The area of saccade endpoint clusters monotonically increased as a function of eccentricity (Fig. 2*C*), in agreement with previous studies (Kowler and Blaser 1995).

Visual and movement response properties

We isolated the responses of 166 neurons (60 in monkey F, and 106 in monkey JL) during the different periods of the task. Figure 3*A* shows the peristimulus time histograms (PSTHs, 50 ms time bins) of an example neuron's (FS2C12U2) activity corresponding to the 40 stimulus locations. In line with previous studies, we observed different visual response profiles among single cells (Fig. 3*C*-*F*) (Suzuki and Azuma 1983; Mikami et al. 1982): phasic activation, tonic activation, phasic-tonic activation, and tonic suppression. We divided the visual period—during which the monkey fixated while a peripheral stimulus appeared—into 'early visual' and 'late visual' epochs to account for the temporal dynamics of the visual response, and to ensure that the visual time window was similar to that for the presaccadic epoch (colors in Fig. 3*B* delineate epochs).

Due to its extensive connections with visual and oculomotor areas within the saccade generation circuit, area 8Ar likely plays a role in visuomotor integration and preparation of saccades. One of our goals was to determine whether the neurons' receptive fields (RFs) and movement fields (MFs) exhibit a Gaussian shape and scale with eccentricity, a trend observed in other visual (Schall 1995) and oculomotor areas (Sparks et al. 1976). We plotted tuning curves—the mean activity across polar angle—for each eccentricity (Fig. 4*A*). We then

302 determined the angular width of tuning from twice the standard deviation of a univariate
303 Gaussian to the peak-centered tuning curve at each eccentricity (Fig. 4*A, inset*). Figure 4*B* shows
304 that RF and MF width scale positively as a function of eccentricity (Kruskal-Wallis test, $P <$
305 0.05).

306 It has been reported that RFs in area 8Ar tend to be large—ranging from 10 x 10 to 60 x
307 60 degrees visual angle (dva) (Mikami et al. 1982)—and show a bias for the contralateral visual
308 hemifield (Suzuki and Azuma 1983). Figure 5*A* shows the RFs measured during the early and
309 late epochs of visual stimulation and the MF of two example neurons. The spatial extent of both
310 fields was very similar. We estimated the RF and MF centers from the Cartesian coordinates of
311 the peak of the bivariate Gaussian fit to the activity. We followed the same procedure for all 166
312 of the recorded neurons. We excluded 45 (27%) of the 166 single units that failed to demonstrate
313 significant response modulation compared to baseline in any of the epochs (Fig. 5*B*). Of the
314 neurons that were tuned (n = 121, Kruskal-Wallis test, $P < 0.05$), 68 (56%) were visuomovement
315 cells (tuned in either early visual or late visual and presaccadic epochs); 39 (32%) were visual
316 cells (tuned in either early or late visual epoch); and 14 (12%) were movement cells (tuned in the
317 presaccadic epoch only) (Fig. 5*B*). Of the cells that were visually selective (including visual and
318 visuomovement cells, n=107), 81 (76%) preferred the contralateral visual hemifield; that is, the
319 peak of the Gaussian defining the RF center was contralateral to the recording site. By contrast,
320 only 26 (24%) of the units preferred the ipsilateral hemifield (Fig. 5*C*). This bilateral
321 representation with a contralateral bias agrees with previous studies reporting 42% ipsilateral and
322 58% contralateral preference in the LPFC (Lennert and Martinez-Trujillo 2013). Movement
323 neurons also displayed a preference for the contralateral hemifield, with 10/13 (77%) of

movement fields in the contralateral hemifield compared to 3/13 (23%) in the ipsilateral hemifield (Fig. 5*D*), and one which lay on the meridian.

Suppression below baseline

Whereas most cells exhibited only elevated response in their RF and MF, a subset (n = 15) of visually selective cells had zones of suppression relative to baseline as well as zones of activation above baseline within their RF (Fig. 5*A, second row*). We considered a cell to be *suppressed* if the magnitude of suppression was at least 50% of the peak activation of that cell. We characterized cells exhibiting only activation as *non-suppressed*. The characterization of suppressed cells is such that cells with a low baseline firing rate may not be considered suppressed, as the magnitude of suppression is inevitably limited by the baseline activity. For our purposes, a neuron's "preference" was considered the location of peak activation above baseline, for both suppressed and non-suppressed neurons. For suppressed cells, the zone of suppression was invariably in the anti-preferred location of the cell. Our conservative criteria may under estimate the proportion of suppressed cells; it was intended to avoid false positives.

There was a strong bias for representing the contralateral visual hemifield among non-suppressed cells (Fig. 5*C*). However, a significantly higher proportion (z-score, $P < 0.05$) of suppressed cells preferred the ipsilateral hemifield (9/15; 60%) compared to the proportion of non-suppressed cells preferring the ipsilateral hemifield (17/92; 18%) (Fig. 5*C*). Conversely, only 6/15 (40%) of suppressed cells compared to 75/92 (82%) of non-suppressed preferred the contralateral hemifield. Therefore, suppressed cells tended to have a stronger preference for the ipsilateral hemifield compared to non-suppressed cells.

Receptive field-movement field overlap

We examined whether the RF and the MF of the visuomovement neurons overlap. To this end, we determined the center of the RF (early visual epoch) and MF (presaccadic epoch) and computed the Euclidean distances between them for 17 cells in monkey JL and 30 cells in monkey F. We found that for most cells, the RF and MF centers were located within 4 dva of each other (Fig. 6*A*). However, in some neurons, particularly in monkey F, the field shifted by more than 10 dva from the early visual to the presaccadic epoch. This suggests that in some recorded neurons a complex transformation from visual signals into motor commands make take place.

We also compared the size of the receptive and movement fields. We calculated the elliptical area of the bivariate Gaussian model from the standard deviation along the minor and major axes. There was a significant positive correlation between RF and MF size for the visuomovement neurons of both JL and F (Pearson's correlation, $P < 0.05$) (Fig. 6*B*). There was a tendency, particularly in monkey F, for the movement fields to be slightly larger. We examined whether difference in size was correlated with the magnitude of the field shift and found a poor correlation between the two variables, with a weak correlation in monkey F (Pearson's correlation, $P < 0.05$), and a non-significant correlation in monkey JL (Fig. 6*C*). Our relatively small sample size makes interpretation of these results difficult. Therefore, this question needs to be addressed with a larger sample size in future studies.

Contrast response functions

Whereas the relationship between contrast level and visual response has been thoroughly described in early visual areas, fewer studies have elucidated how contrast is encoded in higher cortical areas, and to our knowledge none have addressed this question in area 8Ar. We examined the contrast response function in representative visual, visuomovement, and movement

cells (Fig. 7*A*). As anticipated, visual and visuomovement (but not movement) cells exhibited a sigmoidal relationship between neural response and contrast level in the early visual epoch with no modulation of response as a function of contrast during the presaccadic epoch. We determined that 19 of 67 (28.4%) visually selective cells in monkey F and 14 of 40 (35.0%) in JL were modulated by contrast ($R^2 > 0.7$) in the early visual epoch (Table 1). From these best fit models of sigmoid function, we determined the distribution of parameters for the contrast response functions of visually selective cells in area 8Ar (Fig. 7*B*). Cells demonstrated a median R_{max} of 18.0 for monkey F, 20.8 for JL; exponent (n) of 2.9 for F and 3.1 for JL; semisaturation constant (C_{50}) of 5.6 for F and 3.9 for JL; and a minimum-contrast response (M) of -1.4 for F and -1.8 for JL (Table 1). The parameter distributions were the same between individuals, save for the C_{50}, which was lower in monkey JL (Table 1; Wilcoxon rank sum, $P < 0.05$). This may reflect individual differences in contrast sensitivity between the two animals. We also examined response latency of contrast-modulated cells (n=33) using Poisson spike train analysis (as detailed in Hanes et al. 1995; Legéndy and Salcman 1985), and plotted these latencies as a function of contrast (Fig. 8). We found that the response latency decreases monotonically as a function of contrast.

Topographic organization of location preference

A hallmark study into the systematic anatomical organization of RF size and eccentricity in the LPFC revealed isocontour lines of these neuronal RF features in the region between the arcuate sulcus and the posterior tip of the principal sulcus (Suzuki and Azuma 1983). Although the systematic organization of unidimensional variables (eccentricity or angle) has been queried, anatomical clustering according to the two-dimensional preferred location has not been described.

The preferred location of an electrode on the array was mapped onto its cortical position according to a two-dimensional spatial color map (Fig. 9*C*). Space was discretized into five eccentricities and four quadrants. Moran's I (spatial autocorrelation) was computed over every unique distance between elements on the array, considering first only the nearest neighbors, and increasing the spatial scale until the entire array was considered. Comparisons of location selectivity on a single electrode with itself (distances of zero) were excluded. Chance values were obtained via permutation test. We randomly shuffled each electrode's spatial preference label (excluding the non-tuned electrodes) 1000 times, taking the 95 percentile range of chance values (Fig. 9*B, grey shaded region*) for comparison with our experimental Moran's I values. The analysis of Moran's I revealed clusters of similar location preference on the cortex up to a spatial scale of 4 mm for monkey JL and 1.5 mm for monkey F (Fig. 9B).

We also analyzed the degree of clustering of neurons according to their preferred angle and eccentricity. We mapped the preferred angle (discretized into quadrants) and the preferred eccentricities onto the arrays according to the respective spatial colormaps (Fig. 10*C*) and applied Moran's I analysis to determine the degree of clustering according to these spatial dimensions. Monkey F did not show any clustering according to angle or eccentricity (Fig. 10*B*). For monkey JL, however, we found that neurons with similar angular preference were clustered between 1 and 4 mm for the early visual epoch, and up to 4 mm for the late visual and presaccadic task epochs (Fig. 10*B*). Taken together, the topographical analysis suggests that neurons with RFs and MFs in similar locations were clustered on the cortical surface.

DISCUSSION

We showed that area 8Ar of the LPFC contains spatial representations of both visual hemifields although biased towards the contralateral visual hemifield. These representations comprise

415 populations of neurons with visual, movement, and visuomovement activity. Neurons within the
416 area have Gaussian-shaped RFs and MFs that scale with eccentricity. The responses of visual
417 and visuomovement neurons are modulated by stimulus contrast. We also observed that neurons
418 with RFs in the ipsilateral hemifield tend to exhibit activity suppressed below baseline when a
419 stimulus is presented in locations opposite to their excitatory RFs. Finally, although area 8Ar
420 receives a multitude of inputs (Yeterian et al. 2012) from retinotopically-organized cortical
421 areas—including the area MT, and V4 (Felleman and Van Essen 1991)— our results do not
422 support the notion that area 8Ar is retinotopic. However, we found clusters of neurons with
423 similar RF locations in both animals during the early period of the visual response.

424 *Response properties of neurons in area 8Ar*

425 Several response profiles have been reported in area 8Ar neuronal populations, including
426 phasic activation, tonic activation, phasic-tonic activation, and tonic suppression (Mikami et al.
427 1982; Suzuki and Azuma 1983). Phasic activation is characterized by a brief surge of discharge
428 shortly (approximately 100 ms) after the appearance of the visual stimulus, after which activity
429 returns to baseline within 750 ms (Mikami et al. 1982). Cells exhibiting tonic activation,
430 however, increase their firing rate and maintain it until the stimulus is removed. Phasic-tonic
431 activation is characterized by a transient surge in firing rate followed by steady discharge lasting
432 the duration of the visual stimulus. Tonic suppression below baseline is apparent in some cells
433 with high baseline firing rate during fixation, and maintains suppression as long as the visual
434 stimulus is presented. In the present study, we observed examples of each of these response
435 profiles (Fig. 3*C*-*F*).

436 It is known that the spatial resolution of vision becomes increasingly coarse moving from
437 the fovea towards the periphery (Spillmann et al. 1987; Schall 1995). One proxy for the decrease

438 in visual acuity towards the periphery is the relationship between RF size and eccentricity, as
439 these two factors have been found to vary systematically and inversely as a function of distance
440 from the fovea across many visual areas (Hubel and Wiesel 1974; but see Dow et al. 1981). This
441 trend results from the high foveal receptor density in the retina, and a gradient drop-off towards
442 the margins. Moreover, because fewer neurons are devoted to representing the visual peripheral,
443 eccentric RFs are larger. Indeed, a positive relationship between the RF size and eccentricity has
444 been demonstrated in area V1 (Van Essen et al. 1984). Cortical magnification is greater in V1
445 compared to area 8Ar (present study); this is reflected in the fact that the small, parafoveal RFs
446 in V1—which range from 0.25-0.75 degrees in diameter (Hubel and Wiesel 1968)—are much
447 smaller than the width of RFs near the fovea in area 8Ar (ranging from approximately 2 - 7
448 degrees) (present study, Fig. 4*B*).

449 We observed large RFs whose width scales with eccentricity (Fig. 4). In contrast to the
450 smaller, Gaussian RFs in early visual areas, RFs of area 8Ar neurons tend to be elongated and
451 extend across multiple eccentricities. It is possible that RF shapes in this area are more complex
452 than reported here; with our mapping stimulus, it is difficult to estimate the exact shape of these
453 RFs (e.g., deviation from a Gaussian shape or the existence of multiple excitatory and inhibitory
454 fields). In interpreting Gaussian fits one must take into account the sampling resolution of the
455 current method. The Gaussian model estimated the peripheral boundaries with less certainty than
456 at more foveal locations, because the probe resolution decreases in the periphery. This occurs as
457 a trade-off between sampling resolution and the parameters tested, such as location and contrast
458 level. Sampling resolution in the periphery was reduced in order to ensure enough trials for each
459 condition (40 locations with 5 contrast levels). This sampling method guarantees sufficient trials

for the analysis of neuronal responses but has the disadvantage of a non-homogenous sampling of eccentricities.

One issue that makes it difficult to fully characterize the RF profiles of these neurons is that RFs in this area can change dynamically under different conditions. For example, RFs in extrastriate, parietal and prefrontal areas such as MT (Womelsdorf et al. 2008), V4 (Tolias et al. 2001), LIP (Ben Hamed et al. 2001) and the LPFC (Lennert and Martinez-Trujillo 2013) have been shown to change depending on task type. In the current study, we have used a limited set of stimuli and a relatively simple task, thus, our results in terms of RF and MF profiles may change under different task conditions.

We categorized neurons according to their visual, movement, and visuomovement activity. Visual cells are considered those with significant activity in response to visual stimuli, but not preceding a saccade; movement cells discharge immediately preceding a saccade, and visuomovement cells discharge in response to visual stimuli as well as immediately preceding a saccade, according to the criteria established by Bruce and Goldberg (1985). We focused on presaccadic activity, as opposed to postsaccadic activity, as we were interested in the signal preceding saccade execution, which may contribute to saccade planning. We found that, of the 166 isolated neurons, 45 (27%) did not respond to the stimulus or in preparation for a saccade. Of the cells exhibiting significant modulation (n=121), we found 68 (56%) visuomovement neurons, 39 (32%) visual neurons, and 14 (12%) movement neurons (Fig. 5*B*). These results are in agreement with those of Takeda and Funahashi (2002) who recorded from single neurons within the periprincipal region of the LPFC, rostral to area 8Ar, during an oculomotor delayed-response task. They found that 86% of neurons encoded visual stimulus location (visual cells), and 13% encoded the saccade location (movement cells). Although the exact proportion of cells

with visual, movement, or visuomovement tuning is difficult to determine with single cell recordings, due to sampling bias, these studies strongly suggest that visuomovement cells are the most frequently encountered type, followed by visual and movement cells.

Hemifield representation bias

A bias for representation of the contralateral hemifield in saccade-related and visual activity is common amongst many visual and oculomotor areas. For example, presaccadic neurons within the FEF overwhelmingly prefer saccades towards the contralateral hemifield (Bruce and Goldberg 1985). Indeed, there has been reported a bias for contraversive saccades among saccade-related neurons in LIP (Patel et al. 2010), the SEF (Schlag and Schlag-Rey 1987), in the SC (Sparks and Mays 1980), and in the periprincipalis region of the LPFC (Funahashi et al. 1991).

In the present study, we found that 81 (76%) of visually selective cells (n = 107) preferred the contralateral hemifield, compared to 26 (24%) ipsilaterally-preferring cells (Fig. 5*C*). Lennert and Martinez-Trujillo (2013) sampled populations of neurons in area 8Ar and in the anteriorly-adjacent area 9/46 and observed a proportion of 58% neurons preferring contralateral and 42% preferring ipsilateral visual targets, indicating that as one moves rostrally within the LPFC, the representation of the visual field may become less biased towards the contralateral hemifield.

Visual information from the ipsilateral hemifield necessarily crosses the midline via the corpus callosum at some point along the visual processing stream. There is callosal input onto the LPFC from the homotopic area of the opposite hemifield (Goldman-Rakic and Schwartz 1982) as well as sensory and association areas (Barbas et al. 2005). Recent work by Lennert and Martinez-Trujillo (2013) has indicated that ipsilateral and contralateral neurons may play a

different role in target selection. The response profiles of the neurons in the same task differ depending on the relevance of the stimulus in the RF. These authors proposed that contralateral neurons seem to be more engaged in target selection, while ipsilateral neurons seem to be more engaged in sustaining attention on a target once it has been selected. However, to fully clarify this issue, one must extend the results of these studies to a variety of tasks and RF mapping methods that go beyond the scope of the present study.

Contrast response functions

It has been suggested that higher order cortical areas represent more complex stimulus features (Maunsell and Newsome 1987); it is unclear to what extent these areas allocate resources to encode simpler stimulus features, e.g. contrast. In comparison to neurons in early visual areas, the neurons in higher order areas tend to have a lower semi-saturation constant (C_{50}), and thus higher contrast sensitivity. For instance, macaque LGN and V1 neurons have demonstrated a median C_{50} of 0.11-0.5 and 0.33, respectively (Sclar et al. 1990). By contrast, MT neurons display a strikingly lower median C_{50} value of 0.07 (7% contrast normalized to 1.0) (Sclar et al. 1990). Similarly, area 8Ar neurons exhibit a low median C_{50} of 4-6% contrast (present study, Table 1). Although comparisons between studies is difficult due to different methods of measuring luminance contrast and different display features, our results suggest that neurons in area 8Ar have sigmoid contrast response functions and contrast sensitivity similar to neurons in early visual areas.

The distribution of latencies as a function of contrast in our sample, also follow a well-described trend (Albrecht et al. 2002) for latencies to be shorter at higher contrast values (Fig. 8). Our results suggest that visually selective neurons in 8Ar inherit their contrast sensitivity from visual neurons.

529 *Topographical organization*

530 An outstanding question is whether RFs of neurons in area 8Ar of the lateral prefrontal
531 cortex show a defined topography (e.g., retinotopy). Previous studies have suggested anatomical
532 clustering of neurons with similar response properties (Suzuki and Azuma 1983; Kiani et al.
533 2015) in the PFC. Indeed, Kiani and colleagues (2015) recorded from microelectrode arrays
534 implanted on the prearcuate convexity in a very similar location to our implantation site. They
535 sampled a number of locations in the visual field and observed RF and MF profiles
536 (Supplemental Fig. S9) similar to those found in the current study (Fig. 5*A*), and conducted a
537 comparison of RF similarity which mirrors our analysis of RF and MF overlap (Fig. 6).

538 However, differences in recording techniques may render a comparison between previous
539 studies and the current study difficult. In the case of Suzuki and Azuma (1983), the location of
540 penetrations with single electrodes are difficult to analyze since the brain may change in volume
541 during the experiments due to repeated injuries of blood vessels in the region, edema, and dural
542 thickening. In our case, the use of chronically-implanted multielectrode arrays and intraoperatory
543 pictures allows for a fixed reference system where the topography of RFs and MFs can be
544 analyzed relative to the position of the neurons on the cortical surface and to fixed landmarks
545 that are visible after dura mater opening (e.g., the arcuate sulcus). Nonetheless, recording with
546 multielectrode arrays may also have some limitations; namely, arrays sample neurons from a
547 fixed cortical layer parallel to the array plane, neurons could be sampled twice in different days,
548 and there is a fixed area of 4 x 4 mm where samples are taken from.

549 Our results quantitatively demonstrate that groups of neurons with RFs in similar
550 locations were anatomically clustered (Fig 9*B*), with a slight trend for the upper contralateral
551 visual field to be represented in the ventrolateral portion of the array, and the lower contralateral

552 visual field to be represented in the dorsomedial part of the array (Fig 9*C*). Indeed, these results
553 agree with those of Savaki et al. (2014) who utilized [^{14}C] deoxyglucose quantitative
554 autoradiography to examine activity in the prefrontal cortex of macaques during saccades.
555 Similar to the present investigation, they found a dorsal to ventral gradient within area 8Ar
556 representing the contralateral lower to upper visuo-oculomotor space. Taken together, these
557 findings indicate a topographic arrangement of visuo-oculomotor space within area 8Ar.

558 In the present study, area 8Ar RFs were typically large and eccentric (Fig. 5*A*). This is in
559 concordance with previous reports of neurons in the region between the principal sulcus and the
560 arcuate sulcus (the middle arcuate area) having large, somewhat eccentric RFs (Suzuki and
561 Azuma 1983). Suzuki and Azuma (1983) recorded from the prearcuate cortex spanning from the
562 inferior to the superior limb of the arcuate sulcus, and reported a trend for smaller foveal and
563 parafoveal RFs in the inferior portion of the prearcuate cortex, in the approximate location of
564 area 45 (Petrides and Pandya 1999). There is a topographic organization of increasing RF size
565 moving from the inferior towards the middle arcuate area (Suzuki and Azuma 1983). Thus the
566 population of neurons spanning the prearcuate cortex—bounded dorsally by area 8B and
567 ventrally by area 45—likely contains a complete map of eccentricities, and the present study
568 samples from the portion of the map representing an intermediate range of eccentricities
569 (~15dva).

570 Although we examined clustering according to eccentricity (Fig. 10*B*), we did not observe
571 the isocontour lines of RF eccentricity reported by Suzuki and Azuma (1983). This could be
572 attributed to the fact that our clustering algorithm was less sensitive to the geometry of a line, or
573 the fact that the current study mapped eccentricity out to 15 dva, whereas Suzuki and Azuma
574 (1983) mapped a much larger range of eccentricities (out to 60 dva). Furthermore, Suzuki and

575 Azuma (1983) used *Macaca mulatta* whereas the present study uses *Macaca fascicularis*,
576 therefore the different results may be ascribed to species differences.

577 Although, similar to the FEF, area 8A contains the visual and motor spatial representation
578 of a visual and saccadic target, this area may show functional differences compared to its
579 caudally-adjacent neighbor (the FEF). For instance, we find clustering of neurons representing
580 the vector angle of saccades (Fig. 10*B*), whereas in the FEF, there is topographic organization of
581 the saccadic amplitude but not angle (Bruce et al 1985; Stanton et al 1989). Nevertheless, this
582 finding was only clearly present in one animal, thus this issue needs to be examined in more
583 detail using a larger sample size (number of animals) and homogenous mapping procedures
584 across areas.

585 The difference in spatial representation (foveal vs peripheral representation) recapitulates the
586 cytoarchitectonically-defined prefrontal areas, although functional borders appear to be gradual.
587 Area 45 receives projections from the inferotemporal cortex area TEO (Webster et al. 1994)
588 representing central vision, whereas medial area 8Ar receives input from the posterior parietal
589 cortex (Yeterian et al. 2012), representing peripheral vision (Motter and Mountcastle 1981;
590 Schall 1995). This trend of central to peripheral, ventrolateral to dorsomedial RF eccentricity in
591 the prearcuate gyrus corresponds to the trend of small-amplitude saccades in ventrolateral
592 portion of the FEF, and large-amplitude saccades in the dorsomedial FEF (Bruce et al. 1985).

593 One interesting finding in our study is that the two neuronal populations of the animals show
594 different tendencies to cluster, at least in respect to the degree of clustering. Clusters of neurons
595 preferring similar location in the visual field seem to be larger and better-defined in monkey JL
596 compared to monkey F (Fig. 9). This difference may be the result of individual variability
597 between animals, e.g., patterns that are intrinsic to each individual according to the interplay

between genetically determined connectivity and the effect of environmental stimulation. Alternatively, this variability may be a feature of the prefrontal cortex that is not found in visual areas, and may reflect the sole effect of environmental variables on the wiring of the LPFC. Since previous studies have reported that when animals are trained in a motion direction task, neurons in area 8Ar are selective for motion direction (Mendoza-Halliday et al. 2014), we tend to support the latter hypothesis (selectivity shaped by learning experience). It is impossible to answer this question with our data; however, the fact that we found such differences in topographical organization between animals opens new questions and hypotheses regarding the role of the PFC in individual variability in cognitive skills.

Cells suppressed by visual stimulus at the antipreferred direction

Some visually selective cells in the FEF have been reported to show suppression when a saccade was prepared towards a visual target presented outside the RF (Burman and Segraves 1994), particularly when the target was presented in the hemifield contralateral to that cell's RF (Schall et al. 1995a). Within the LPFC, there have been reports of cells with activity suppressed below baseline in a restricted portion of the visual field (Mikami et al. 1982). We also characterized a subset of cells with a zone of brisk suppression in the location opposite the zone of activation (Fig. 5*A*), and there was a bias for these suppressed cells to have RF and MF peak activation in the ipsilateral hemifield (Fig. 5*C*).

Recent studies suggest that, during target selection, populations of prefrontal neurons compete or cooperate for preferential processing of a visual stimulus. To this point, during target selection, pairs of FEF neurons with overlapping RFs coordinate by firing in synchrony when a target is placed within the overlapping portion of the RFs. By contrast, neurons with non-overlapping RFs compete, firing out of synchrony when the target appears in the RF of one

neuron but not the other (Cohen et al. 2010). In the present study, suppressed cells tended to have zones of activation in the ipsilateral hemifield (Fig. 5*C*). Some proportion of neurons with contralateral RFs likely suppresses activity of ipsilaterally-preferring cells via inhibitory interneurons. These inhibitory circuits may mediate biased competition (Desimone and Duncan 1995) between hemispheres.

Differences and similarities between area 8Ar and FEF

There are a few functional differences in the properties of neurons in area 8Ar reported here and those of neurons in the FEF reported by other studies. It should be noted that many of the studies of the FEF include recordings spanning both the prearcuate gyrus and the rostral bank of the arcuate sulcus, making it difficult to differentiate the response properties between FEF and 8Ar. Visually responsive cells in the FEF are usually not feature-selective, although it has been reported that with training, some cells can gain feature selectivity (Bichot et al. 1996). By contrast, neurons in area 8Ar demonstrate feature selectivity in sustained activity during a delayed match-to-sample task (Mendoza-Halliday et al. 2014). Finally, the sensory neurons in the FEF tend to strongly prefer the contralateral visual hemifield (Schall 1991), whereas visually selective neurons in area 8Ar display a greater degree of bilateral representation, with a bias towards the contralateral hemifield (Fig. 5*C*). There appears to be no sharp delineation in response properties in FEF and area 8Ar, but rather a gradient of function moving rostrally.

Considered together, these data suggest that area 8Ar and the FEF may play functionally distinct roles in executive processes involved in the generation of saccades, with the FEF more directly linked to saccade execution. However, the function and connectivity of these two areas are intimately linked; thus they likely work in coordination to select a target for saccades. For example, injection with retrograde tracer horseradish peroxidase reveals afferent projections to

644 the SC originating in both the FEF (within the anterior bank of the arcuate sulcus) and area 8Ar
645 (on the prearcuate gyrus) (Fries 1984). One possibility is that area 8Ar is more involved in
646 integrating different types of signals including sensory, reward value, attention, working memory
647 and others, while the FEF is more involved in generating the final gaze command to direct the
648 eyes in space towards objects of interest. The precise mechanism of this process will be
649 addressed by future studies.

650 CONCLUSIONS

651 Area 8Ar displays visual and saccade-related activity and shares connections with a
652 multitude of visual and oculomotor areas. We found that area 8Ar contains populations of visual,
653 movement, and visuomovement neurons with RFs and MFs representing both visual hemifields,
654 and that some of the visually selective neurons were modulated by increasing contrast levels.
655 Therefore, we conclude that area 8Ar likely plays a role in visuomotor integration in preparation
656 for saccades. Future studies are necessary to elucidate the mechanism whereby area 8Ar
657 integrates visual information to influence saccade target selection. Although the topographic
658 organization of the LPFC (particularly retinotopy) remains uncertain, we have demonstrated that
659 neurons with similar RF and MF locations are anatomically clustered within an area of 4x4 mm
660 of 8Ar, particularly with respect to RF location during the early periods of visual stimulation.

661 AKNOWLEDGEMENTS

662 This work was supported by grants to J.C.M.-T. from the NSERC, EJLB foundation, CIHR, and
663 Canada Research Chair program. We would like to thank Mr. Stephen Nuara and Mr. Walter
664 Kucharski for technical support in conducting this experiment. We would also like to thank our
665 lab members for their thoughtful critique and comments in preparation of this manuscript.

DISCLOSURES

The authors declare no conflict of interest.

REFERENCES

Albrecht DG, Geisler WS, Frazor RA, Crane AM. Visual cortex neurons of monkeys and cats: Temporal dynamics of the contrast response function. *J Neurophysiol* 88: 888-913, 2002.

Albrecht DG, Hamilton DB. Striate cortex of monkey and cat: contrast response function. *J Neurophysiol* 48: 217–237, 1982.

Andersen RA, Asanuma C, Essick G, Siegel RM. Corticocortical connections of anatomically and physiologically defined subdivisions within the inferior parietal lobule. *J Comp Neurol* 296: 65–113, 1990.

Arcaro MJ, Pinsk MA, Li X, Kastner S. Visuotopic organization of macaque posterior parietal cortex: An fMRI study. *J Neurosci* 6: 2064-2078, 2011.

Bahill AT, Clark MR, Stark L. The main sequence, a tool for studying human eye movements. *Math Biosci* 24: 191–204, 1975.

Barbas H, Hilgetag CC, Saha S, Dermon CR, Suski JL. Parallel organization of contralateral and ipsilateral prefrontal cortical projections in the rhesus monkey. *BMC Neurosci* 6: 32, 2005.

Barbas H, Mesulam MM. Organization of afferent input to subdivisions of area 8 in the rhesus monkey. *J Comp Neurol* 200: 407–431, 1981.

Barone P, Joseph JP. Role of the dorsolateral prefrontal cortex in organizing visually guided behavior. *Brain Behav Evol* 33: 132–135, 1989.

Ben Hamed S, Duhamel JR, Bremmer F, Graf W. Representation of the visual field in the

lateral intraparietal area of macaque monkeys: a quantitative receptive field analysis. *Exp Brain Res* 140: 127-144, 2001.

Bichot NP, Schall JD, Thompson KG. Visual feature selectivity in frontal eye fields induced by experience in mature macaques. *Nature* 381: 697–699, 1996.

Blatt GJ, Andersen RA, Stoner GR. Visual receptive field organization and cortico-cortical connections of the lateral intraparietal area (area LIP) in the macaque. *J Comp Neurol* 299: 421–445, 1990.

Bruce CJ, Goldberg ME. Primate frontal eye fields. I. Single neurons discharging before saccades. *J Neurophysiol* 53: 603-633, 1985.

Bruce CJ, Goldberg ME, Bushnell MC, Stanton GB. Primate frontal eye fields. II. Physiological and anatomical correlates of electrically evoked eye movements. *J Neurophysiol* 54: 714–734, 1985.

Burman DD, Segraves MA. Primate frontal eye field activity during natural scanning eye movements. *J Neurophysiol* 71: 1266–1271, 1994.

Cohen JY, Crowder EA, Heitz RP, Subraveti CR, Thompson KG, Woodman GF, Schall JD. Cooperation and competition among frontal eye field neurons during visual target selection. *J Neurosci* 30: 3227–3238, 2010.

Desimone R, Duncan J. Neural mechanisms of selective visual attention. *Annu Rev Neurosci* 18: 193–222, 1995.

Dow BM, Snyder AZ, Vautin RG, Bauer R. Magnification factor and receptive field size in foveal striate cortex of the monkey. *Exp Brain Res* 44: 213–228, 1981.

Van Essen DC, Maunsell JH, Bixby JL. The middle temporal visual area in the macaque: myeloarchitecture, connections, functional properties and topographic organization. *J*

712 *Comp Neurol* 199: 293-326, 1981.
713 **Van Essen DC, Newsome WT, Maunsell JHR.** The visual field representation in striate cortex
714 of the macaque monkey: Asymmetries, anisotropies, and individual variability. *Vision Res*
715 24: 429–448, 1984.
716 **Everling S, Tinsley CJ, Gaffan D, Duncan J.** Filtering of neural signals by focused attention in
717 the monkey prefrontal cortex. *Nat Neurosci* 5: 671–6, 2002.
718 **Felleman DJ, Van Essen DC.** Distributed hierarchical processing in the primate cerebral cortex.
719 *Cereb Cortex* 1: 1–47, 1991.
720 **Fries W.** Cortical projections to the superior colliculus in the macaque monkey: a retrograde
721 study using horseradish peroxidase. *J Comp Neurol* 230: 55-76, 1984.
722 **Funahashi S, Bruce CJ, Goldman-Rakic PS.** Neuronal activity related to saccadic eye
723 movements in the monkey's dorsolateral prefrontal cortex. *J Neurophysiol* 65: 1464–1483,
724 1991.
725 **Gattass R, Sousa AP, Gross CG.** Visuotopic organization and extent of V3 and V4 of the
726 macaque. *J Neurosci* 8: 1831–1845, 1988.
727 **Genovesio A, Brasted PJ, Mitz AR, Wise SP**. Prefrontal cortex activity related to abstract
728 response strategies. *Neuron* 47: 307–20, 2005.
729 **Goldman-Rakic PS, Schwartz ML.** Interdigitation of contralateral and ipsilateral columnar
730 projections to frontal association cortex in primates. *Science* 216: 755–757, 1982.
731 **Hair JF, Sarstedt M, Ringle CM, Mena JA.** An assessment of the use of partial least squares
732 structural equation modeling in marketing. *J Acad Market Sci* 40: 414–433, 2012.

Hanes DP, Thompson KG, Schall JD. Relationship of presaccadic activity in frontal eye field and supplementary eye field to saccade initiation in macaque: Poisson spike train analysis. *Exp Brain Res* 103: 85-96, 1995.

Hubel DH, Wiesel TN. Receptive fields and functional architecture of monkey striate cortex. *J Physiol* 195: 215-243, 1968.

Hubel DH, Wiesel TN. Uniformity of monkey striate cortex: a parallel relationship between field size, scatter, and magnification factor. *J Comp Neurol* 158: 295–305, 1974.

Khayat PS, Niebergall R, Martinez-Trujillo JC. Attention differentially modulates similar neuronal responses evoked by varying contrast and direction stimuli in area MT. *J Neurosci* 30: 2188–97, 2010.

Kiani R, Cueva CJ, Reppas JB, Newsome WT. Dynamics of neural population responses in prefrontal cortex indicate changes of mind on single trials. *Curr Biol* 24: 1542–1547, 2014.

Kiani R, Cueva CJ, Reppas JB, Peixoto D, Ryu SI, Newsome WT. Natural Grouping of Neural Responses Reveals Spatially Segregated Clusters in Prearcuate Cortex. *Neuron* 85: 1359–1373, 2015.

Kowler E, Blaser E. The accuracy and precision of saccades to small and large targets. *Vision Res* 35: 1741–1754, 1995.

Leavitt ML, Pieper F, Sachs A, Joober R, Martinez-Trujillo JC. Structure of spike count correlations reveals functional interactions between neurons in dorsolateral prefrontal cortex area 8a of behaving primates. *PLoS ONE* 8: e61503, 2013.

Legéndy CR, Salcman M. Bursts and recurrences of bursts in the spike trains of spontaneously active striate cortex neurons. *J Neurophysiol* 53: 926-939, 1985.

Lennert T, Martinez-Trujillo J. Strength of response suppression to distracter stimuli determines attentional-filtering performance in primate prefrontal neurons. *Neuron* 70: 141–52, 2011.

Lennert T, Martinez-Trujillo JC. Prefrontal neurons of opposite spatial preference display distinct target selection dynamics. *J Neurosci* 33: 9520–9, 2013.

Martínez-Trujillo JC, Treue S. Attentional modulation strength in cortical area MT depends on stimulus contrast. *Neuron* 35: 365–370, 2002.

Maunsell JH, Van Essen DC. The connections of the middle temporal visual area (MT) and their relationship to a cortical hierarchy in the macaque monkey. *J Neurosci* 3: 2563–2586, 1983.

Maunsell JHR, Newsome WT. Visual processing in monkey extrastriate cortex. *Annu Rev Neurosci* 10: 363–401, 1987.

Maynard EM, Nordhausen CT, Normann RA. The Utah Intracortical Electrode Array: A recording structure for potential brain-computer interfaces. *Electroencephalogr Clin Neurophysiol* 102: 228–239, 1997.

Mendoza-Halliday D, Torres S, Martinez-Trujillo JC. Sharp emergence of feature-selective sustained activity along the dorsal visual pathway. *Nat Neurosci* 17: 1255–1262, 2014.

Michelson AA. *Studies in Optics*. Chicago: University of Chicago Press, 1927.

Mikami A, Ito S, Kubota K. Visual response properties of dorsolateral prefrontal neurons during visual fixation task. *J Neurophysiol* 47: 593–605, 1982.

Miller EK. The prefrontal cortex: Complex neural properties for complex behavior. *Neuron* 22: 15–17, 1999.

Moran PAP. Notes on continuous stochastic phenomena. *Biometrika* 37: 17–23, 1950.

Motter BC, Mountcastle VB. The functional properties of the light-sensitive neurons of the posterior parietal cortex studied in waking monkeys: foveal sparing and opponent vector organization. *J Neurosci* 1: 3–26, 1981.

Normann RA, Maynard EM, Rousche PJ, Warren DJ. A neural interface for a cortical vision prosthesis. *Vision Res* 39: 2577–2587, 1999.

Patel GH, Shulman GL, Baker JT, Akbudak E, Snyder AZ, Snyder LH, Corbetta M. Topographic organization of macaque area LIP. *Proc Natl Acad Sci USA* 107: 4728–4733, 2010.

Petrides M, Pandya DN. Dorsolateral prefrontal cortex: comparative cytoarchitectonic analysis in the human and the macaque brain and corticocortical connection patterns. *Eur J Neurosci* 11: 1011–36, 1999.

Preuss TM, Goldman-Rakic PS. Myelo- and cytoarchitecture of the granular frontal cortex and surrounding regions in the strepsirhine primate *Galago* and the anthropoid primate *Macaca*. *J Comp Neurol* 310: 429-474, 1991.

Rossi AF, Bichot NP, Desimone R, Ungerleider LG. Top down attentional deficits in macaques with lesions of lateral prefrontal cortex. *J Neurosci* 27: 11306–11314, 2007.

Savaki HE, Gregoriou GG, Bakola S, Moschovakis AK. Topography of Visuomotor Parameters in the Frontal and Premotor Eye Fields. *Cereb Cortex* 25: 3095-3106, 2014.

Schall JD, Hanes DP, Thompson KG, King DJ. Saccade target selection in frontal eye field of macaque. I. Visual and premovement activation. *J Neurosci* 15: 6905–6918, 1995.

Schall JD, Morel A, King DJ, Bullier J. Topography of visual cortex connections with frontal eye field in macaque: convergence and segregation of processing streams. *J Neurosci* 15: 4464–4487, 1995.

Schall JD. Neural basis of saccade target selection. *Rev. Neurosci.* 6: 63–85, 1995.

Schall JD. Neuronal activity related to visually guided saccades in the frontal eye fields of rhesus monkeys: comparison with supplementary eye fields. *J Neurophysiol* 66: 559-579, 1991.

Schlag J, Schlag-Rey M. Evidence for a supplementary eye field. *J Neurophysiol* 57: 179–200, 1987.

Sclar G, Maunsell JH, Lennie P. Coding of image contrast in central visual pathways of the macaque monkey. *Vis Res* 30: 1–10, 1990.

Seo H, Barraclough DJ, Lee D. Dynamic signals related to choices and outcomes in the dorsolateral prefrontal cortex. *Cereb Cortex* 17 (suppl 1): i110-i117, 2007.

Sparks DL, Holland R, Guthrie BL. Size and distribution of movement fields in the monkey superior colliculus. *Brain Res* 113: 21–34, 1976.

Sparks DL, Mays LE. Movement fields of saccade-related burst neurons in the monkey superior colliculus. *Brain Res* 190: 39–50, 1980.

Spillmann L, Ransom-Hogg A, Oehler R. A comparison of perceptive and receptive fields in man and monkey. *Hum Neurobiol* 1: 51-62, 1987.

Stanton GB, Bruce CJ, Goldberg ME. Topography of projections to the frontal lobe from the macaque frontal eye fields. *J Comp Neurol* 330: 286–301, 1993.

Stanton GB, Deng SY, Goldberg ME, McMullen NT. Cytoarchitectural characteristic of the frontal eye fields in macaque monkeys. *J Comp Neurol* 282: 415–427, 1989.

Suzuki H, Azuma M. Topographic studies on visual neurons in the dorsolateral prefrontal cortex of the monkey. *Exp Brain Res* 53: 47–58, 1983.

Takeda K, Funahashi S. Prefrontal task-related activity representing visual cue location or

saccade direction in spatial working memory tasks. *J Neurophysiol* 87: 567–588, 2002.

Tolias AS, Moore T, Smirnakis SM, Tehovnik EJ, Siapas AG, Schiller PH. Eye movements modulate visual receptive fields of V4 neurons. *Neuron* 29: 757-767, 2001.

Tremblay S, Pieper F, Sachs A, Martinez-Trujillo J. Attentional Filtering of Visual Information by Neuronal Ensembles in the Primate Lateral Prefrontal Cortex. *Neuron* 85: 202-15, 2015.

Ungerleider LG, Desimone R. Cortical connections of visual area MT in the macaque. *J Comp Neurol* 248: 190–222, 1986.

Wallis JD, Anderson KC, Miller EK. Single neurons in prefrontal cortex encode abstract rules. *Nature* 411: 953–956, 2001.

Webster MJ, Bachevalier J, Ungerleider LG. Connections of inferior temporal areas TEO and TE with parietal and frontal cortex in macaque monkeys. *Cereb Cortex* 4: 470–483, 1994.

Wegener SP, Johnston K, Everling S. Microstimulation of monkey dorsolateral prefrontal cortex impairs antisaccade performance. *Exp Brain Res* 190: 463–473, 2008.

Wise SP, Murray EA, Gerfen CR. The frontal cortex-basal ganglia system in primates. *Crit Rev Neurobiol* 10: 317–356, 1996.

Womelsdorf T, Anton-Erxleben K, Treue S. Receptive field shift and shrinkage in macaque middle temporal area through attentional gain modulation. *J Neurosci* 36: 8934-8944, 2008.

Yeterian EH, Pandya DN, Tomaiuolo F, Petrides M. The cortical connectivity of the prefrontal cortex in the monkey brain. *Cortex* 48: 58–81, 2012.

Zuur AF, Ieno EN, Smith GM. Analyzing Ecological Data. 2007.

FIGURE CAPTIONS

FIG. 1. Recording site and visually guided saccade task. *A*: Recording site. A microelecrode array (MEA) was implanted in the left area 8Ar of each monkey, posterior to the posterior end of the principal sulcus (PS), and anterior to the arcuate sulcus (AS). Schematic shows cytoarchitectonic delineations of area 8Ar and neighboring prefrontal areas identified by Preuss and Goldman-Rakic 1991 and Yeterian et al. 2012. Photographs show recording site for monkeys JL (top) and F (bottom) relative to the sulci labeled in the schematic. Orientation legend: C, caudal; D, dorsal; R, rostral; V, ventral. *B*: Timeline of visually guided saccade task. After 650 ms of fixation, a peripheral sine wave grating appears at one of 40 locations arranged along eight polar angles (45 degree intervals) and five eccentricities (3 dva intervals); white dotted circles indicate possible stimulus locations. Monkey maintains central fixation for 650 ms, and at 1300 ms monkey is cued to saccade to the stimulus upon extinguishing the central fixation point. Monkey receives juice reward upon successfully shifting gaze to target.

FIG. 2. Saccade kinematics and saccade precision for subjects JL (left) and F (right). Only saccade endpoints from hit trials are included. *A*: Saccade duration as a function of eccentricity. Duration was calculated from the eye velocity trace as the time from when the velocity first exceeded the threshold (25 deg/s) to when it returned to threshold. *B*: Saccade peak velocity as a function of eccentricity. *C*: Saccade endpoint spread as a function of eccentricity. The spread of the saccade endpoint clusters is derived from the area of the ellipse fit to the cluster of endpoints at each target location.

FIG. 3. Task epochs and example single unit activity (neuron FS2C12U2). *A*: Peristimulus time histograms (PSTHs) represent the single unit responses over the time course of an entire trial at

the 40 different locations. *B*: Task epochs superimposed on a PSTH of activity at a single location, highlighted in *A*. *C*-*F*: Visual response profiles of representative neurons. PSTHs were plotted at the location of the RF center. Shown here are the response profiles of neurons exhibiting *C*: tonic activation, *D*: phasic-tonic activation, *E*: phasic activation, and *F*: tonic suppression. Bin width is 50 ms. Visual activity (after stimulus onset, before saccade cue) is shown in black. Abscissa: time in milliseconds. Ordinate: response rate in spikes per second.

FIG. 4. Width of tuning across eccentricities. *A*: Single neuron FS2C12U2 tuning curves for each eccentricity plotted for the different task epochs: the early visual (left), late visual (middle), and presaccadic (right). *Inset*: A univariate Gaussian fit to the tuning curve for each eccentricity. The angular width of tuning is determined from the standard deviation (σ) of the Gaussian model at each eccentricity. *B*: Population receptive and movement field width as a function of eccentricity. Fill colors correspond to the eccentricities depicted in *A*.

FIG. 5. Receptive and movement fields. *A*: Receptive fields (RF; early and late visual epochs) and movement fields (MF; presaccadic epoch) for example non-suppressed neuron (top row) and suppressed neuron (bottom row). A two-dimensional Gaussian is fit to the mean baseline-subtracted activity at the 40 locations; values between stimulus locations are interpolated. Firing rate relative to baseline represented by colorbar. *B*: Population visuomotor tuning. Horizontal bars show the proportion of visual (V), visuomovement (VM), and movement (M) neurons. Tuned neurons refer to the proportion of neurons with significant task-related activity (ANOVA, $P < 0.05$). Grey section represents the proportion of neurons without selectivity during any of the task epochs. *C*: Percentage of neurons with preferred locations in the contralateral (blue) compared to the ipsilateral (red) visual hemifield among all visually selective—visual and

visuomovement—neurons (left), non-suppressed neurons (middle), and suppressed neurons (right). D: Percentage of movement neurons preferring the ipsilateral (red) and contralateral (blue) hemifield.

FIG. 6. Receptive and movement field overlap. *A:* Distribution of field shifts from receptive field (RF) to movement field (MF). The magnitude of the field shift was given by the Euclidean distance (in dva) between the center of the RF and MF of each visuomovement neuron in monkeys JL (left) and F (right). *B:* Correlation between RF and MF size. Size was determined as the area of the elliptical perimeter of the two dimensional Gaussian. Pearson's correlation (r) reported in lower right corner. Significant ($P < 0.05$) correlations denoted with an asterisk. *C:* Correlation between field size difference and field shift. The difference in size (MF_{area}-RF_{area}) is plotted against the magnitude of the field shift.

FIG. 7. Contrast response functions. *A:* Mean response relative to baseline depicted for example visual (left), visuomovement (middle), and movement (right) neurons during the early visual (black trace) and presaccadic (grey trace) epochs at the location of peak activity. The dotted lines connect mean firing rate for each contrast level and solid lines represent the best fit function (either a sigmoid function if $R^2 > 0.7$ or a line through the mean activity); error bars depict SEM across all trials presented at that contrast level. Inset tables display the parameter values for the sigmoid function fit to the data, as well as the goodness of fit (R^2). *B:* Parameter values for contrast response functions of visually selective cells. The cumulative distributions of parameters (R_{max}, n, C_{50}, M) for monkeys F and JL are represented by grey bars and black bars, respectively. The optimized parameters were determined by the sigmoid model fits (R^2 >0.7).

FIG. 8. Visual response latency as a function of contrast levels. Box plots represent the visual response latencies of all contrast-modulated neurons (n=33) from both subjects as a function of contrast level. The visual response latency relative to stimulus onset was calculated using Poisson spike train analysis applied to all trials at each contrast levels.

FIG. 9. Anatomical clustering of preferred location across task epochs. *A*: Schematic illustrating position of array implants in monkeys JL (left) and F (right) relative to the principal (PS) and arcuate (AS) sulci. For *C*, arrays shown in *A* are rotated clockwise until parallel to the horizontal. *B*: Magnitude of clustering of preferred location. Solid grey line depicts the spatial autocorrelation (Moran's I; metric of clustering) calculated over increasing spatial scales. Grey shaded area represents 95% range of chance values. Positive values indicate clustering of similar values; zero indicates random spatial organization; negative values indicate spatial segregation of similar values. Grey dotted line indicate the extent of significant clustering. *C*: Preferred locations mapped onto array. Preferred location—defined as the location of the peak of the Gaussian model fit to the thresholded activity on an electrode ($R^2 > 0.5$) —was mapped onto the array according to a two-dimensional spatial colormap (see inset). Grey channels are non-tuned; black channels are ground electrodes.

FIG. 10. Anatomical clustering as a function of angle and eccentricity. *A:* Schematic illustrating position of array implants. *B:* Magnitude of clustering (Moran's I) as a function of angle (red) and eccentricity (blue). Dotted lines of each colors indicate the extent of significant clustering for each spatial dimension. *C*: Preferred angle (top row) and eccentricity (bottom row) mapped onto array according to their respective colormaps. Grey channels are non-tuned; black channels are ground electrodes.

935 Table 1. Median parameter values of contrast response functions fit to activity of contrast-
936 modulated neurons. Asterisks indicates significantly different values between monkeys JL and F
937 for a given parameter (Wilcoxon rank sum, $P < 0.05$).

938

939

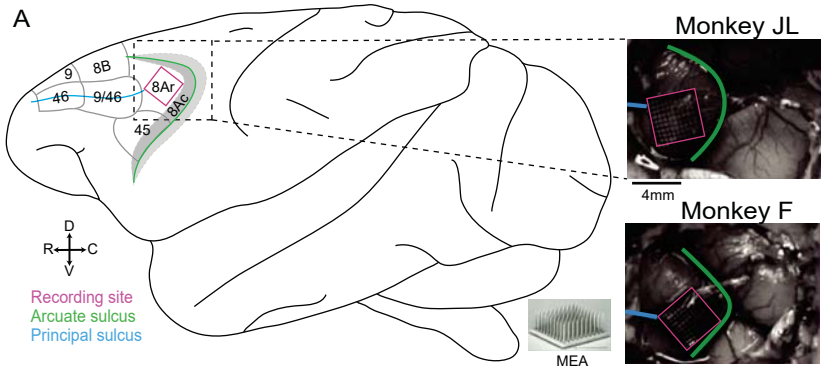
A
Monkey JL
9
8B
46
9/46
8Ar
8Ac
45
4mm
Monkey F
D
R
C
V
Recording site
Arcuate sulcus
Principal sulcus
MEA
B
Time(ms)
0
650
1300
1500
eye position

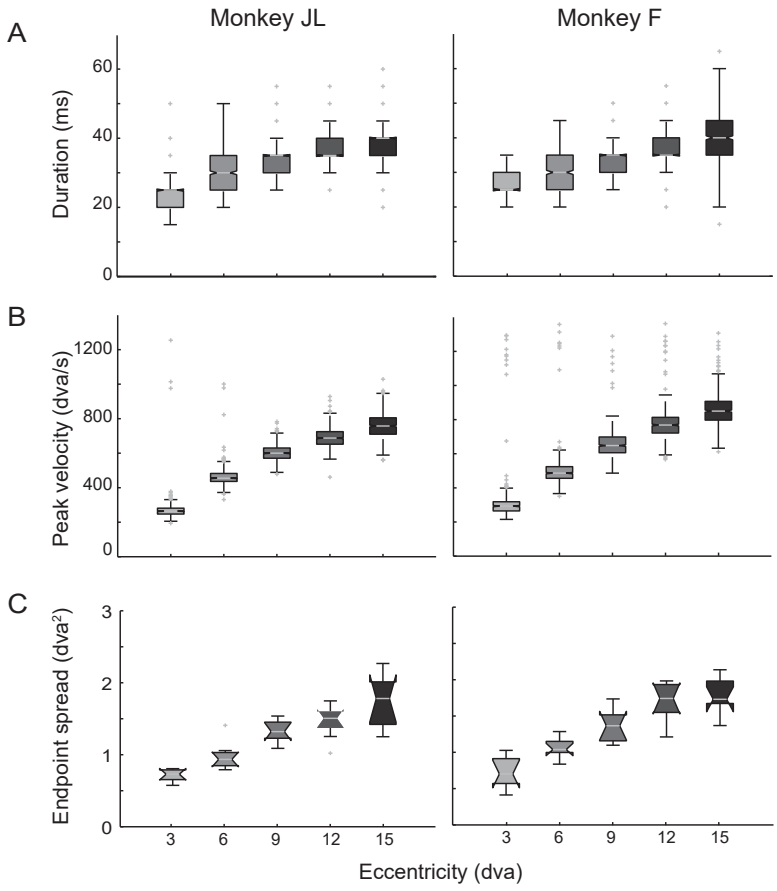
A
Monkey JL
Monkey F
Duration (ms)
0
20
40
60
B
Peak velocity (dva/s)
0
400
800
1200
C
Endpoint spread (dva²)
0
1
2
3
3
6
9
12
15
Eccentricity (dva)

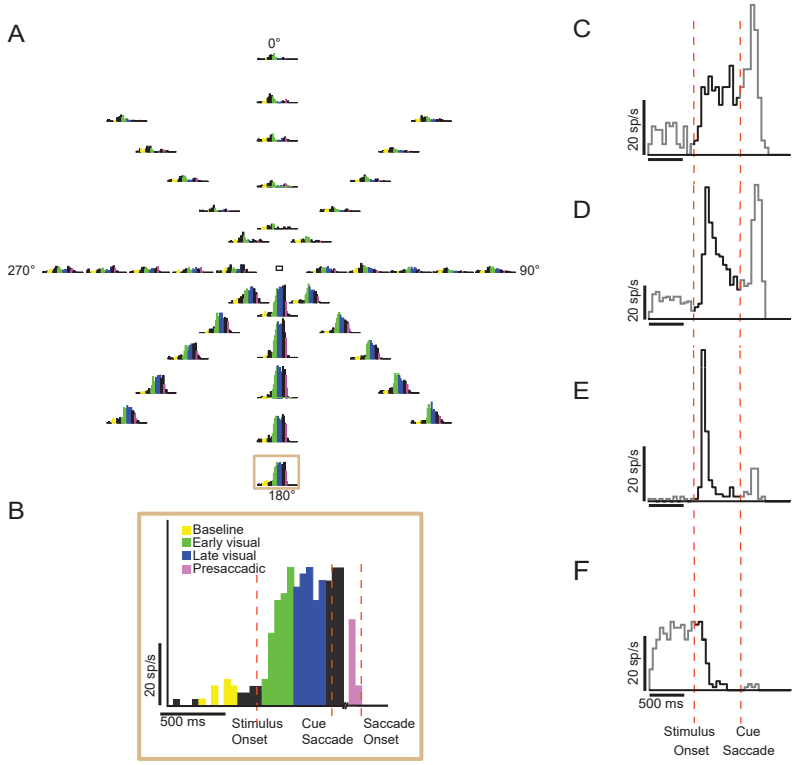
A
0°
270°
90°
180°
B
Baseline
Early visual
Late visual
Presaccadic
20 sp/s
500 ms
Stimulus Onset
Cue
Saccade
Saccade Onset
C
D
E
F
20 sp/s
500 ms
Stimulus Onset
Cue Saccade

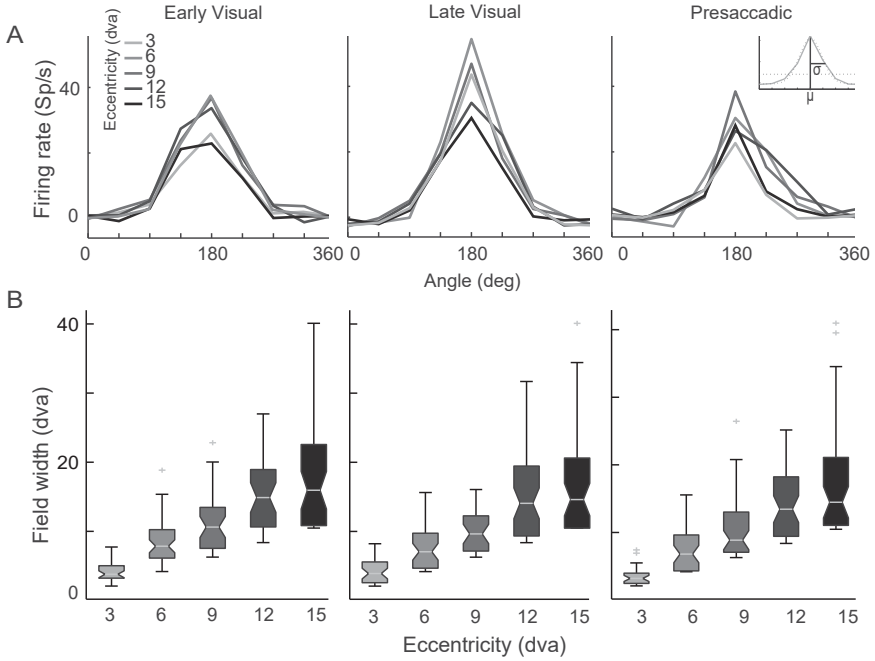
A
Early Visual
Late Visual
Presaccadic
Eccentricity (dva)
3
6
9
12
15
Firing rate (Sp/s)
40
0
0
180
360
σ
μ
Angle (deg)
B
Field width (dva)
40
20
0
3
6
9
12
15
Eccentricity (dva)

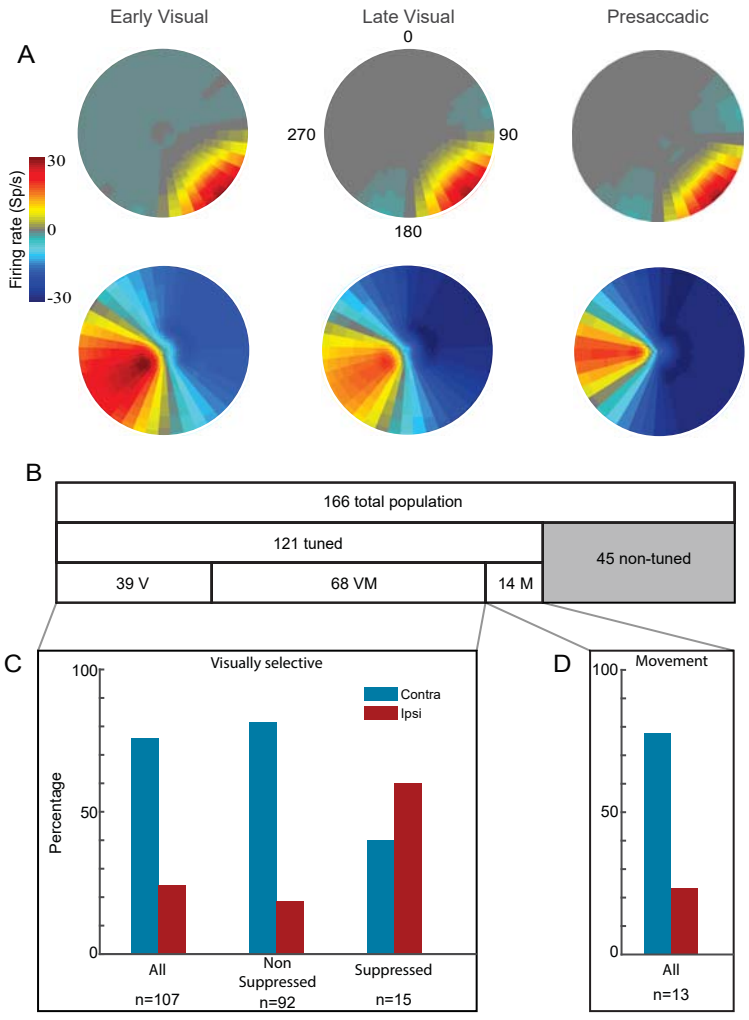
A
Early Visual
Late Visual
Presaccadic
0
270
90
180
Firing rate (Sp/s)
30
0
-30
B
166 total population
121 tuned
45 non-tuned
39 V
68 VM
14 M
C
Visually selective
Contra
Ipsi
Percentage
100
50
0
All
n=107
Non Suppressed
n=92
Suppressed
n=15
D
Movement
100
50
0
All
n=13

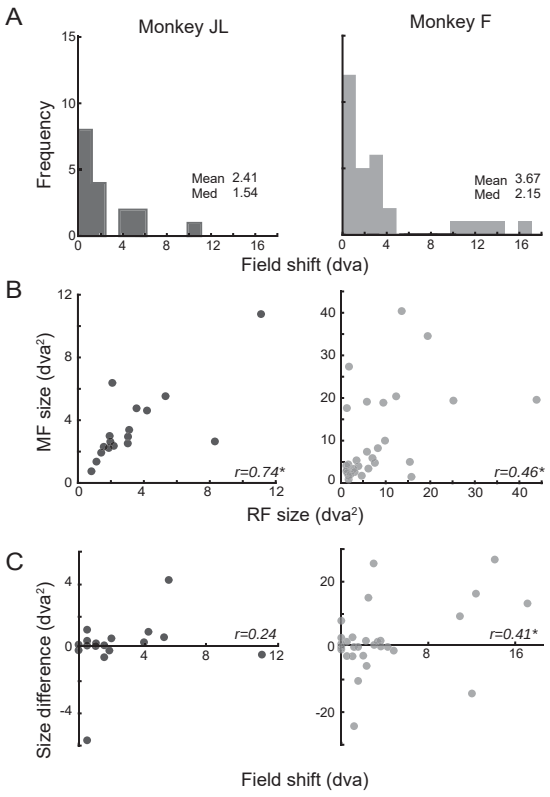
A
Monkey JL
Monkey F
Frequency
Mean 2.41
Med 1.54
Mean 3.67
Med 2.15
Field shift (dva)
B
MF size (dva²)
r=0.74*
r=0.46*
RF size (dva²)
C
Size difference (dva²)
r=0.24
r=0.41*
Field shift (dva)

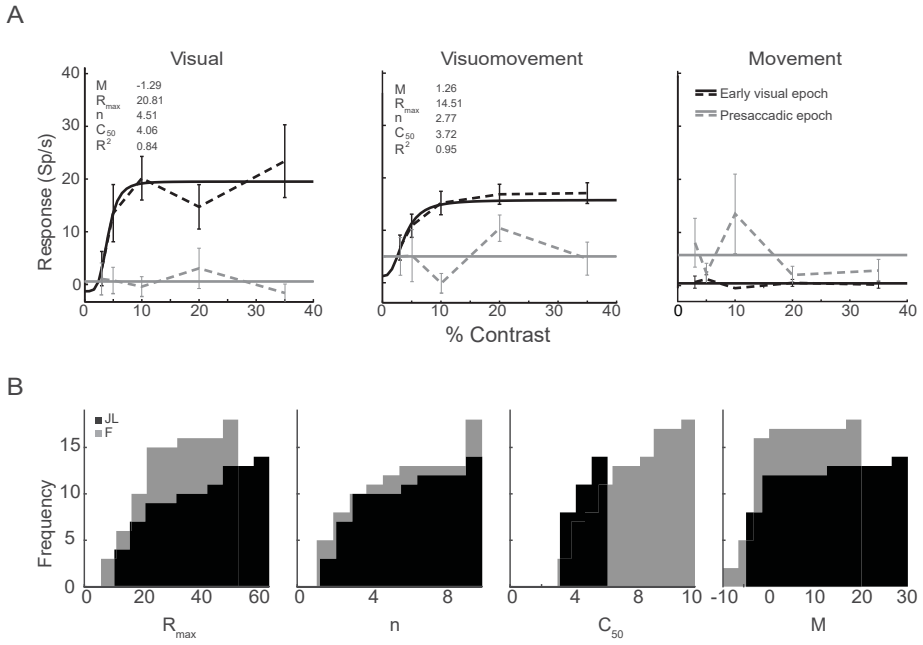
A
Visual
Visuomovement
Movement
M -1.29
Rmax 20.81
n 4.51
C50 4.06
R2 0.84
M 1.26
Rmax 14.51
n 2.77
C50 3.72
R2 0.95
Early visual epoch
Presaccadic epoch
Response (Sp/s)
% Contrast
B
JL
F
Frequency
Rmax
n
C50
M

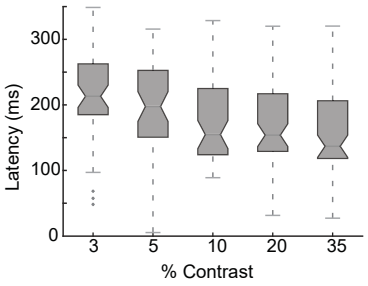
300
200
100
0
Latency (ms)
3
5
10
20
35
% Contrast

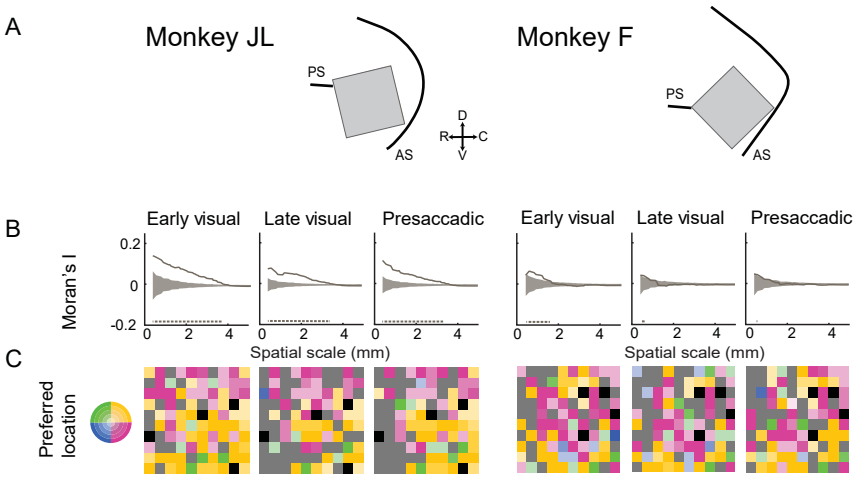
A
Monkey JL
PS
AS
D
R
C
V
Monkey F
PS
AS
B
Early visual
Late visual
Presaccadic
Early visual
Late visual
Presaccadic
Moran's I
0.2
0
-0.2
0
2
4
Spatial scale (mm)
Spatial scale (mm)
C
Preferred location

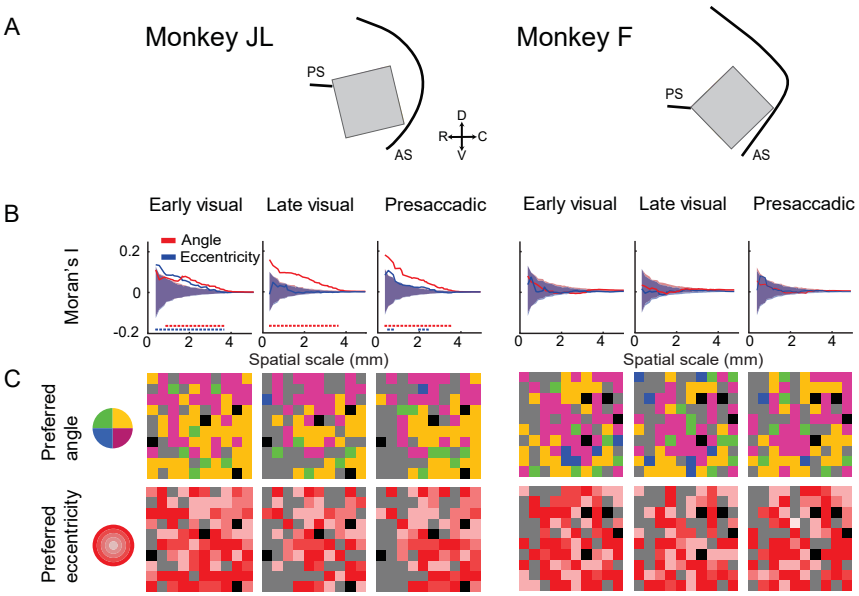
A
Monkey JL
PS
AS
D
R
C
V
Monkey F
PS
AS
B
Early visual
Late visual
Presaccadic
Early visual
Late visual
Presaccadic
Moran's I
Angle
Eccentricity
0.2
0
-0.2
0
2
4
Spatial scale (mm)
Spatial scale (mm)
C
Preferred angle
Preferred eccentricity

Subject	(units)	R_{max}	n	C_{50}	M
JL	14	20.8	3.1	3.9	-1.8
F	19	18.0	2.9	5.7 *	-1.4